*Full Paper*

# Supercapacitive Properties of Europium Oxide Nanoparticles Decorated on Nitrogen Doped Graphene Nanosheets Hybridized with Lanthanum based Metal-Organic Frameworks

**Hamed Pourfarzad,[1] and Farshad Torabi[2]**

*[1]Center of Excellence in Electrochemistry, University of Tehran, Tehran, Iran*
*[2]Department of Mechanical Engineering, K.N. Toosi University of Technology, Tehran, Iran*

*Corresponding Author,
E-Mail: h.pourfarzad2030@gmail.com

**Abstract**- In this research, a new nanocomposite as supercapacitor based on the europium oxide ($Eu_2O_3$) nanoparticles decorated on the nitrogen doped graphene nanosheets (EuNs@NGNs) hybridized with the metal-organic framework of lanthanum and 1,5-naphthalene disulfonic acid ligand (La-MOF) were synthesized. The design of experiment (DOE) method and Design Expert software was used to study the influence and optimize the structural effects for the studied nanocomposite. The structural characteristics of the supercapacitive material were investigated with XRD, FTIR and Raman techniques. Also, morphology was evaluated through FESEM and TEM analyses. The electrochemical profile of these materials in a three-electrode setup was investigated using cyclic voltammetry (CV), galvanostatic charge-discharge (GCD) and electrochemical impedance spectroscopy (EIS) techniques. The suitable electrolyte for this supercapacitor is 6.0 M sodium hydroxide solution. The specific capacitances of the EuNs@NGNs, La-MOFs and EuNs@NGNs /La-MOF electrodes were calculated to be 328, 505 and 920 and $F.g^{-1}$ at 2 mV/s. Moreover, EuNs@NGNs /La-MOF had a large energy density (59.62 Wh $kg^{-1}$) at 1511 W $kg^{-1}$and maintained its specific energy (37.09 Wh $kg^{-1}$) even when specific powers as high as (20000 W $kg^{-1}$) were applied. The material also enjoys unique cycling performance and its retention rate after 2500 charge-discharge cycles was determined to be 96.15%.

**Keywords-** Supercapacitive nanocomposite; Europium oxide nanoparticles; Nitrogen-doped graphene nanosheets; Lanthanum-based metal-organic frameworks; Continuous cyclic voltammetry

## 1. INTRODUCTION

Developing efficient materials for energy storage applications is an inevitable need for modern life [1-3]. On the other hand, supercapacitors (SCs) are among the most appealing energy storage devices given their unparalleled qualities including considerable power density and life cycles, and fast delivery rate [4]. SCs are mainly classified as electric double-layer capacitors (EDLCs) and pseudo-capacitors [5-9], the former being based on are carbonaceous materials like nanotubes or graphene, while the latter comprises of electrodes based on noble and transition metal oxides or conducting polymers[7,10]. Accordingly carbon-based materials [11-13], metal oxides and hydroxides [14-20], LDH materials [21] and conducting polymers [22] have been widely studied for SC applications. The possibility of developing cost-effective and processable synthesis and production methods in the case of carbon and conducting polymer-based materials, oxides of transition metals and metal organic frameworks (MOFs) have made the materials the topics of various studies on supercapacitors applications [23-27].

The carbon-based electrode materials offer advantages of thermal and chemical stability considerable conductivity, and large surface area [5]. Among the various carbon-based compounds, reduced graphene oxide (RGO), is a low cost yet highly attractive material [28]. However, there is an incremental demand for high surface area materials capable of rapidly transporting electrons and ions and electrons, which can create stable electrode/electrolyte interfaces.

MOF are a class of candidates for constructing SC electrodes, given their controllable porosity, considerable surface area, and favorable characteristics [29], including the presence of redox-active metal centers [30,31]. However MOF-based materials suffer from poor conductivity and cycling stability, which limits their applicability in SCs [30,32,33]. Accordingly, modification of metal-organic frameworks and their hybridization with conductive materials has turned into an area of research in material science [34-36]. One option is hybridizing MOFs with graphene-based materials. Further to their great electron and charge transfer properties, the large surface area of these carbon-based materials allows for efficient anchoring of MOFs [37-39] forming improved hybrid structures offering the favorable properties of both ingredients.

Another strategy is loading various nanomaterials including transition metal and rare earth oxides (e.g. $MnO_2$, $Mn_3O_4$, $RuO_2$, $CeO_2$, $Yb_2O_3$) on to the carbon based substrates [40-42]. Rare earth compounds have long been used in various catalysts and SC applications given their unique electronic, optical and electrochemical properties [43]. The synthesis of one-dimensional $Eu_2O_3$ nanostructures, has been a recent advance, since it has enhanced the packing density and a number of the active sites in the product as compared with bulk materials [44].

In this work, for the first time we have synthesis $Eu_2O_3$ nanoparticles (EUNs) decorated on nitrogen doped graphene nanosheets (NGNs) hybridized with La-MOF. In the synthesis of

europium oxide nanoparticles and nanocomposites, sonochemical method was used at controlled temperature. The resulting material (EuNs@NGNs/La-MOF) offered improved superapacitive properties compared to similar recent works.

## 2. EXPERIMENTAL

### 2.1. Materials

Carbon black, methanol, isopropyl alcohol, lanthanum nitrate, graphite flake, polyvinylidene fluoride, 6-water europium nitrate salt, phosphoric acid, potassium permanganate, sodium sulfate, potassium hydroxide, sulfuric acid solution, hydrogen peroxide and 1 and 5 naphthalene disulfonic acid were used in the study. All materials were obtained from Merck, Sigma and Aldrich were used as received.

### 2.2. Synthesis of EuNs@NGNs

Nitrogen-doped graphene was prepared using GO, which was obtained using graphite powder in a modified version of Hummer procedure [45]. The process typically involved adding 2 g of graphite powder to 200 ml of an 8/1 mixture of concentrated sulfuric acid and phosphoric acid. While stirring the solution, 10 g of potassium permanganate was added and the reaction mixture was cooled to 20 °C. Next, the mixture was heated to 60 °C and kept under stirring at this temperature for 12 hours, before cooling to ambient conditions, followed by adding 200 g of ice containing 6 ml of 30% oxygenated aqueous solution to yield a light-yellow solution. After separating the solid product, it was repeatedly washed using a 5% hydrochloride solution, and next with water and ethanol. The mixture was eventually dried at 80 °C in vacuum. Next a GO mixture and melamine was prepared and mixed as follows. 130 mg of melamine was added to 15 ml of water, followed by adding 40 mL of graphene oxide to obtain a 1:1 melamine/graphene mixture, which was then subjected to sonication to reach even distribution before drying. 100 mg of the dried sample was placed in a crucible at a temperature of about 430 °C in air for three hours to obtain the final product [46].

In order to synthesize the nanostructure of europium oxide, a sonochemical method was used. First, a solution of europium nitrate was prepared by dissolving some of the europium oxide powder in nitric acid in an ultrasonic device. This solution was then diluted by adding ethanol and 20% aqueous polyvinyl alcohol, before heating to 90°C followed by 120 minutes of vigorous stirring. It was then obtained by compressing the hydroxyl lattice by losing water to a dense porous gel. The gel was then desiccated at 110°C in an oven and next calcined at 400 °C in a to obtain europium oxide [47].

Europium oxide nanocomposite combined with nitrogen doped graphene (EuNs@NGNs) was prepared by easy chemical ultrasonic method. First, a solution containing 70 mg of nitrogen doped graphene was added to a mixture of 55 mmol of europium oxide nanoparticles

in 70 ml of deionized water. The volume of the mixture was next adjusted to reach 100 ml. The mixture is exposed to the high intensity of ultrasonic waves (580 watts per/20 kHz). During ultrasonic aqueous ammonia solution was added to the mixture in a dropwise manner in 120 minutes. During the synthesis, the temperature of the solution is between 55-65 °C [48]. The synthesis method is summarized in Scheme 1.
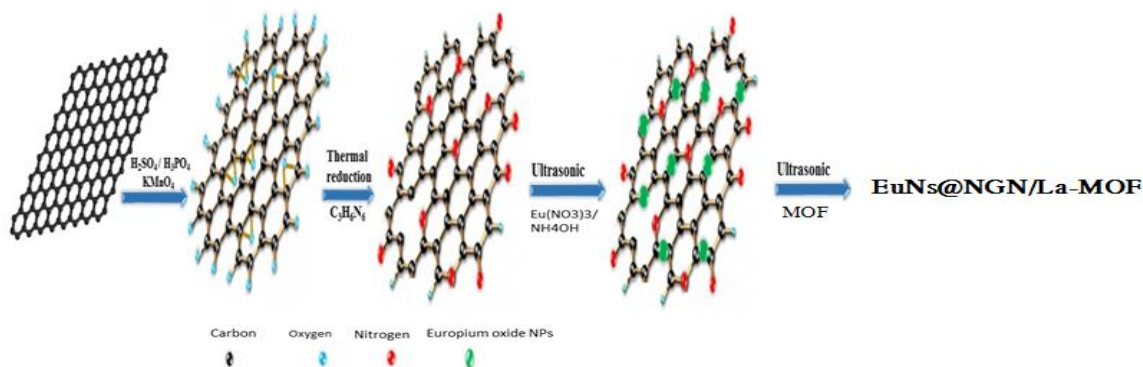


**Scheme 1.** Schematic of the synthesis process of EuNs decorated on NGNs hybridized with La-MOF

### 2.3. Synthesis of MOF using1,5-naphthalene disulfonic acid ligand and lanthanum metal

To synthesize [La(1,5-NDS)$_{1,5}$ (H$_2$O)$_5$] n, 5 ml of water was first poured into a Teflon vessel with a capacity of 23 ml; Then 0.025 mmol of lanthanum nitrate was dissolved in it and 0.025 mmol of 1,5-NDS ligand was added to it and stirred until completely dissolved at room temperature. Finally, 0.02 g of sodium hydroxide was added to adjust the pH at about four, before transferring the mixture to an autoclave and next an oven for thermal treatment at 180 °C for 96 hours. Then, the oven was cooled to the ambient temperature at 1.5 °C/h . Finally, colorless coarse crystals were obtained which were washed with water by centrifugation and clear crystals were prepared for further studies.

### 2.4. Synthesis of EuNs@NGNs/La-MOFs

At this stage, the final composite containing Europium Oxide nanoparticles decorated on N-doped graphene hybridizing with MOF was synthesized by sonochemical method. Initially, 0.25 g of nitrogen doped graphene -europium oxide composite was evenly distributed in 150 ml of water under sonication. Then 20 mg of MOF was dispersed in 10 ml of water and the resulting mixture was added to the nanocomposite container, followed by sonication in a bath at 45 °C for 60 min, and cooling to ambient temperature. The solid product was filtered using a 300 μm filter, washed with water three times before washing with ethanol for another three rounds, and placed in the freezer for 2 days (Scheme 1).

## 2.5. Preparation of the electrodes

To prepare the working electrode, a mixture consisting of 80% by weight of the nanostructured compound of nitrogen doped graphene-europium oxide / MOF, 10% wt. of carbon black (to increase conductivity) and 10% wt. of octyl-methylimidazolium hexafluorophosphate (C6) as sticky agent was mixed and homogenized. Then some of the homogenized mixture was placed on a piece of steel with small cavities as a flow collector and pressed by a press machine at 15 MPa. The surface area of the prepared electrode is around one square centimeter and the weight of the electro-active material obtained by comparing the before and after masses of the steel mesh (about 2 mg; a density of 2 mg per square centimeter). The electrode was then placed in a three-electrode setup to investigate the capacitive behavior.

## 2.6. Characterization

Field emition-scanning electron microscopy (FE-SEM) MIRA3TESCAN-XMU (Czech Republic), and transition electron microscopy (TEM) TEM JEM-2100F (Japan mode) with 200 kV accelerating voltage were used to study the morphology of the material. X-ray diffractometery (XRD, Philips X'pert diffractometer with CuKα radiation ($\lambda = 1.5406$ Å) was also used to evaluate the phase composition of the samples. IR spectra were recorded on an FTIR, Nicolet MagnaIR560 E S.P. Raman spectra was recorded by NRS-5000 Series Raman Spectrometers from JASCO.

## 2.7. Electrochemical measurement

The capacitive behavior of the synthesized nanocomposite, electrochemical studies including CV, GCD, and EIS by three electrodes system including a working nanocomposite electrode, a platinum auxiliary electrode and a silver/silver chloride reference electrode in 6.0 M potassium hydroxide solution were performed. A CHI 660C electrochemical workstation was used for the experiments.

Based on its definition specific capacitance (F g$^{-1}$) can be measured from the equation below:

$$\text{Eq 1:} \qquad C_S = \frac{I\Delta t}{m\Delta V}$$

I, $\Delta t, \Delta V$ and m representing the discharge current (A) and time (sec), the potential window (V) and m mass of the electroactive matter (g).

The discharge scan of CV curves can be used to measure the specific capacitance ($C_s$) using the following expression:

$$\text{Eq 2:} \qquad C_s = (\textstyle\int I \, dv)/(\vartheta m\Delta V)$$

where I, $\Delta V$, $\vartheta$, and m represent current (A), potential window (V), potential sweep rate (V s$^{-1}$) and total mass of the active material present in anode and cathode (g).

The specific energy (E) and power (P) values based on the total mass of the active material for the electrodes are given by:

$$\text{Eq 3:} \qquad Es = \frac{C_{device}\Delta V^2}{2} \times \frac{1000}{3600}$$

$$\text{Eq 4:} \qquad P = \frac{Es}{\Delta t} \times 3600$$

V and $\Delta t$ being the potential window and the discharge time, respectively.

## 2.8. Optimization of composite structure using experimental design

The experimental design method and Design Expert software was used to evaluate the influence and optimal value of the structural factors of the final studied nanocomposite. The studied structural parameters include the amount of doped nitrogen based on the amount of melamine consumed during synthesis, the amount of metal framework and the amount of europium oxide nanoparticles in the composite structure. For this purpose, the five-level Central Composite Design method was used. Based on the calculations, the parameter of nitrogen doping percentage has the most effect and the percentage of europium oxide has the least effect on the capacitance. Also, the percentages of components in EuNs@NGNs/La-MOFs nanocomposite for EuNs nanoparticles, NGNs and MOF are 36, 57 and 7, respectively.

## 3. RESULTS AND DISCUSSION

### 3.1. Evaluation of morphology and structure

Figure 1 shows SEM images for combination of nitrogen-doped graphene nanostructures. As can be seen, nitrogen doped graphene has a folded structure with layers of thin sheets.
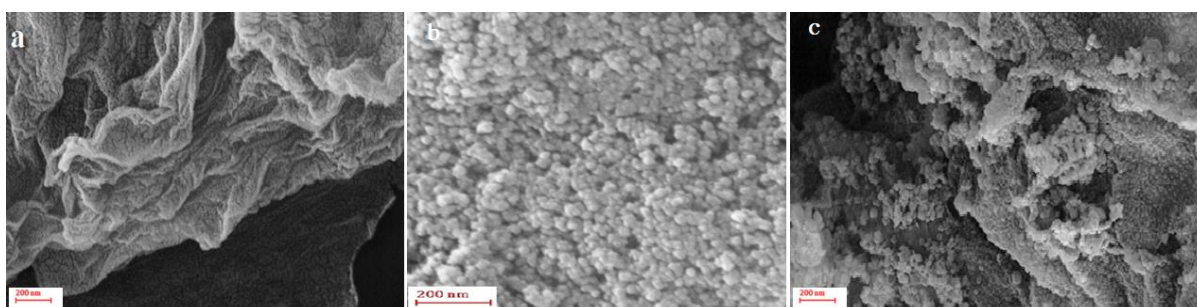


**Figure 1.** FE-SEM images of a) NGNs b) EuNs c) EuNs@NGNs

As it is known, the composition of nitrogen-doped graphene nanostructures is stacked in thin layers as thin as an atom, which indicates the two-dimensional structure of the composition

of N-doped graphene nanostructures with a high surface /volume ratio. The observations well confirmed the results expressed in the previous scientific works [49-52] and indicate the optimal synthesis of nitrogen-doped graphene nanostructures.

Figure 1b shows SEM image of Europium Oxide nanostructure and shows that the size of synthetic nanoparticles is between 20 and 30 nm. However, in order to confirm the placement of Europium Oxide nanoparticles on Nitrogen Doped graphene, to form the EuNs@NGNs/La-MOFs nanocomposite, a transmission electron microscope image is required at different magnifications. Figure 2b clearly shows the TEM images of EuNs@NGNs/La-MOFs nanocomposite. As can be seen from the TEM image, Europium Oxide nanostructures are homogeneously decorated on N-doped graphene layers and the high surface area of the nanostructure, which is among the important parameters in increasing the capacitance of nanostructures can be seen in the image.
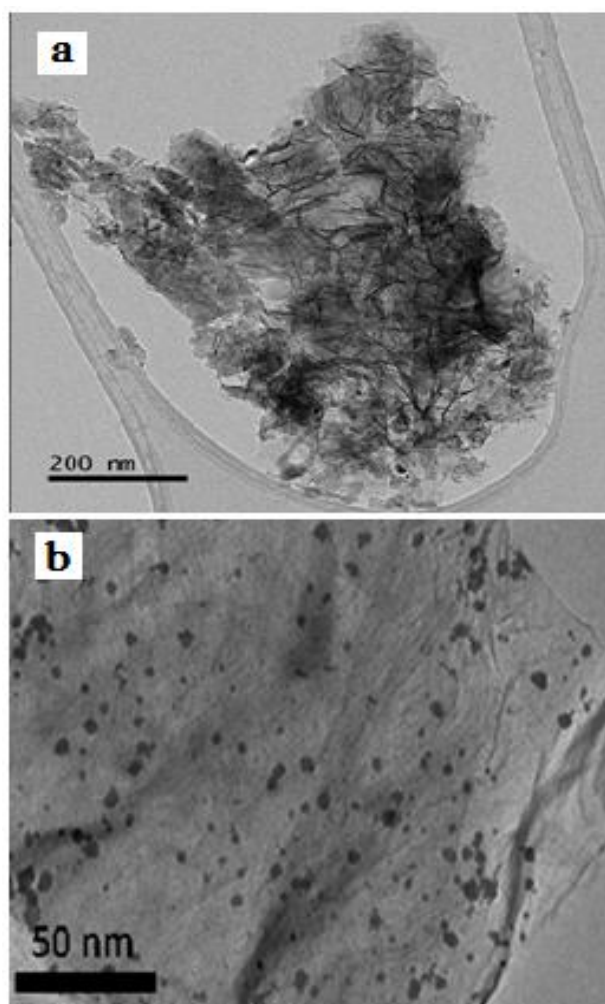


**Figure 2.** TEM images of a) La-MOFs b) EuNs@NGNs/La-MOFs

In the synthesis of lanthanum-organic frameworks, ligand 1,5-naphthalene disulfonic acid was used as an organic binder of the metal salt of lanthanum nitrate as mineral component.

Data from structural analysis of MOF crystals [La (1,5-NDS) $_{1.5}$ (H$_2$O)$_5$]$_n$ were recorded using X-ray single-crystal diffraction. The crystal of this compound is crystallized in the tri-clinic crystal system and the P-1 space group. The lanthanum atom has a coordination number of 9. In this structure, lanthanum is divided into two groups of water, five oxygen atoms from different NDS ligands, eight coordinates. Each of the polyhydra (LnO$_8$) shares an OH-OH edge, which leads to an increase in dimers that are located in the b-direction and connected to the sulfur atoms in the a-direction, as well as the connection in the c-direction by the whole NDS ligand has been established.
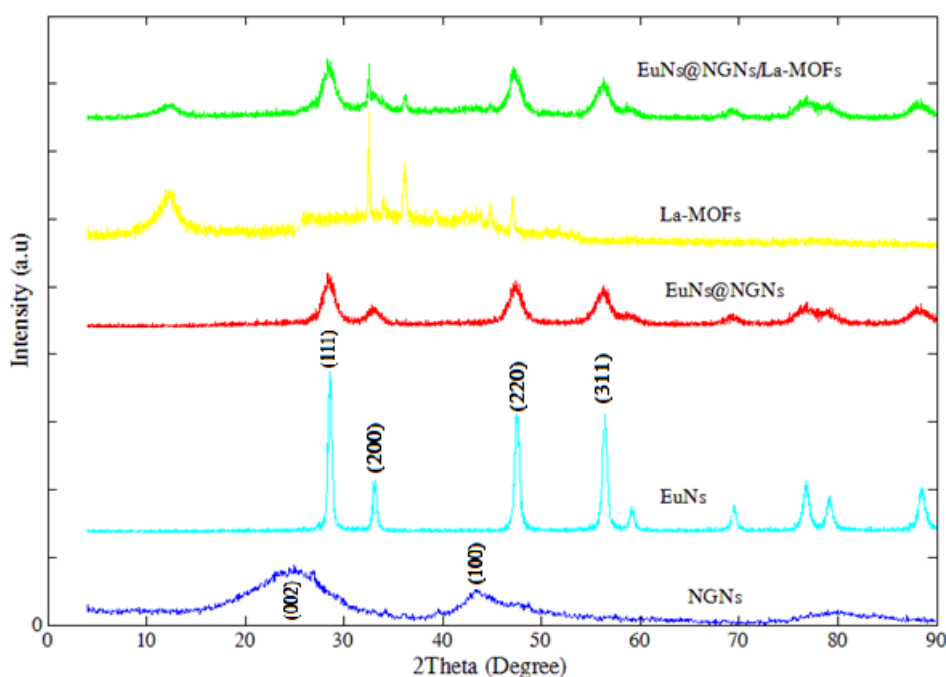


**Figure 3.** X-ray diffraction patterns of NGNs, EuNs, EuNs@NGNs, La-MOFs and EuNs@NGNs/La-MOFs

Figure 3 presents the XRD spectra of NGNs, EuNs, EuNs@NGNs, La-MOFs and EuNs@NGNs/La-MOFs. The respective wide and small peaks at 2θ = 26 ° and 42 ° which correspond to the (002) and (100) planes of graphite-like structures. The lack of a peak at 2θ = 12 ° indicates that graphene oxide is reduced. Peaks in 2θ= 28.58, 33.17, 47.50, 56.41, 59.14, 69.49, 76.80, 79.21 and 88.88 in the patterns indicates the presence of europium oxide nanoparticles and also indicates that europium oxide nanoparticles are properly decorated on nitrogen-doped graphene [53]. The wide noses of the specimens represent the synthesis of crystals with very small dimensions or quasi-crystalline particles. The width of the strips indicates that the synthesized particles are in nanoscale and are more electrochemically active. Figure 4 illustrates the FT-IR spectra for samples of NGNs, EuNs, La-MOFs and EuNs@NGNs/La-MOFs. The signal at 1742 cm$^{-1}$ in the case of N-doped graphene is due to the residues of the C ═ O group due to the graphene oxide reduction process. Which shows

that graphene is well reduced. Absorption bands of about 1160 cm$^{-1}$ and 1032 cm$^{-1}$ are assigned to C-C and C-O. The band 1456 cm$^{-1}$ is related to the C $=$ C and C $=$ N vibrations, reflect the presence of an N-containing group and is in fact a confirmation of nitrogen doping in the reduced graphene oxide structure [54].
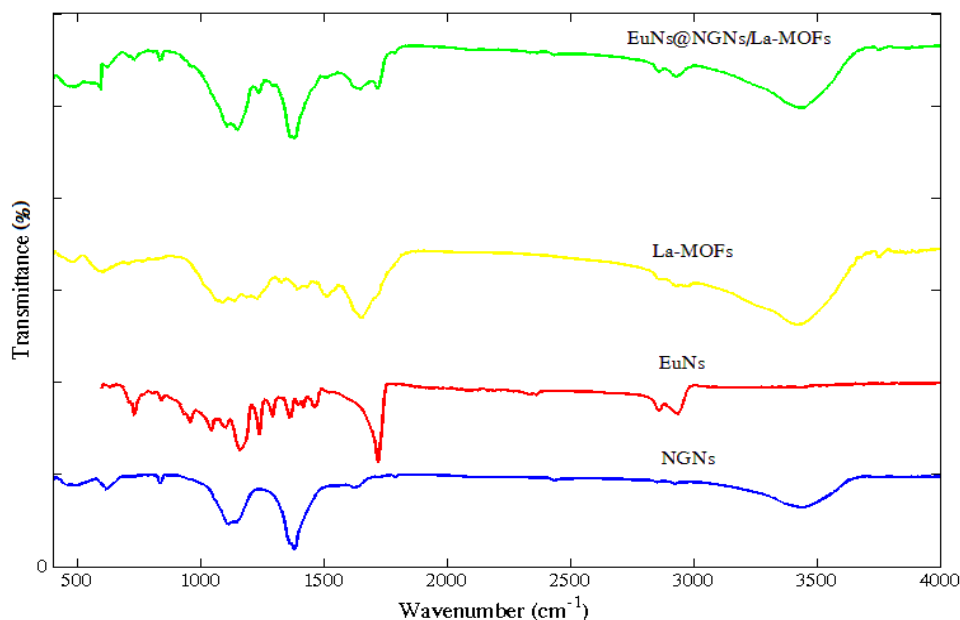


**Figure 4.** FT-IR spectra of NGNs, EuNs, La-MOFs and EuNs@NGNs/La-MOFs
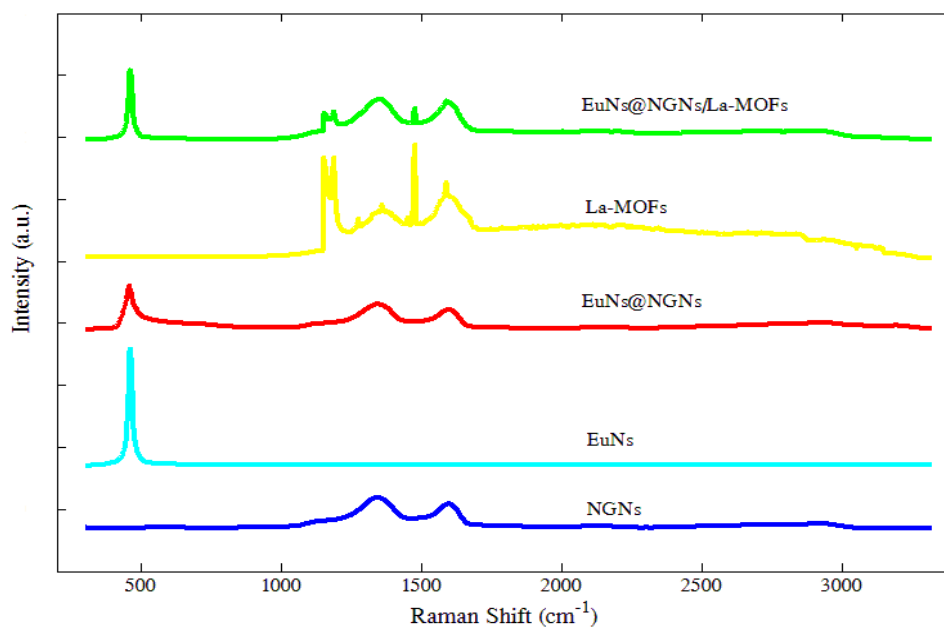


**Figure 5.** Raman shift spectra of NGNs, EuNs, EuNs@NGNs, La-MOFs and EuNs@NGNs/La-MOFs

The FTIR spectra of Europium Oxide nanoparticles and the metal-organic framework synthesized under sonication includes a band at 505 cm$^{-1}$ corresponding to the vibrations of the Europium Oxide crystal. Also, the adsorption bands in 1620 cm$^{-1}$ and 1574 cm$^{-1}$ in the FT-IR spectrum of Europium oxide nanocomposite combined with nitrogen doped graphene and the La-MOF are related to graphene and the interaction of Europium oxide nanoparticles and nitrogen doped graphene is shown in 485 cm$^{-1}$ [55].

Raman spectroscopy is a reliable technique for detecting graphene in its various forms. Raman spectra (figure 5) of carbonaceous materials have certain characteristics in 800-2000 cm$^{-1}$. The G-peak at about 1560 cm$^{-1}$ is related to the E2g photon and the D-peak at about 11360 cm$^{-1}$ reflects the respiration mode of the sp$^2$ atoms that need a defect to emerge, and the graphene without structural defects has a D-peak. Because this Raman mode is only active at the edges of the sheet. The 2D peak (2700 cm$^{-1}$) is the 2$^{nd}$ order of the D band, and is always present in the graphene Raman spectrum even in the absence of the D spectrum because it does not require any structural defects to emerge. The ratios of the intensities of D, G and 2D peaks are often used as a measure of the graphene phase quality. Minimum ID / IG and maximum I2D / IG indicate the best graphite quality [56].

Figure 5 shows the Raman spectroscopic spectra of NGNs, EuNs , EuNs@NGNs, La-MOFs and EuNs@NGNs/La-MOFs samples. As can be seen, nitrogen- doped graphene and europium oxide nanocomposite combined with nitrogen doped graphene have two peaks in 1332 cm$^{-1}$ and 1596 cm$^{-1}$ for the D and G peaks and confirms imperfections and defects in the structure of the carbon materials. The band at 436 cm$^{-1}$ in the spectrum of Europium Oxide nanoparticles and Europium Oxide nanocomposite combined with nitrogen doped graphene is related to the symmetric tensile state between Eu-O$_8$. The band at 460 cm$^{-1}$ with a blue shift indicates the presence of europium oxide nanoparticles present in the material.

## 3.2. Electrochemical experiments

The pseudocapacitive performance and stability profile of EuNs@NGNs, La-MOF and EuNs@NGNs/La-MOF electrodes were evaluated using CV, GCD, and EIS, in a three-electrode cell setup using a 6.0 M solution of KOH in water. Fig. 6a illustrates a comparison of CVs of the MOF, EuNs@NGNs and the EuNs@NGNs/La-MOF electrodes at 25 mV s$^{-1}$ between -0.2 and 0.5 V (vs. Ag/AgCl). **It is clear** that the plots obtained with all electrodes is almost rectangular and quasi-symmetric demonstrating ideal capacitive profiles. Nevertheless, EuNs@NGNs/La-MOF nanocomposite electrodes gave rise to a larger current response and bigger closed area signifying that the nanocomposite has a larger electrochemical active area. This increase in current is due to two effects, Increased electrical conductivity of nitrogen dop graphene due to the increase of europium oxide nanostructures and Synergistic effect of nitrogen dop graphene and europium oxide nanostructures and also the presence of metal-organic MOF framework structure. Reversibility is a key electrochemical factor affecting the

power and capability SC instruments. Hence, EuNs@NGNs/La-MOF nanocomposite electrodes were evaluated in this regard through examining the cyclic voltammograms in different ranges of scanning rates (Figure 6b). As anticipated, with EuNs@NGNs/La-MOF electrodes the specific current rises with the scan rate, which indicates the favorable rate capability. Also, the rectangular shape and symmetry in the cyclic voltammetric diagram for this electrode shown in the Figure 6b indicate good reversibility of the specimen in the said range. In the MOF sample, cyclic voltammetry shows an electrochemical reaction at a potential of 0.1 volt. It can be said that this reaction is an electron transfer between MOF structures.
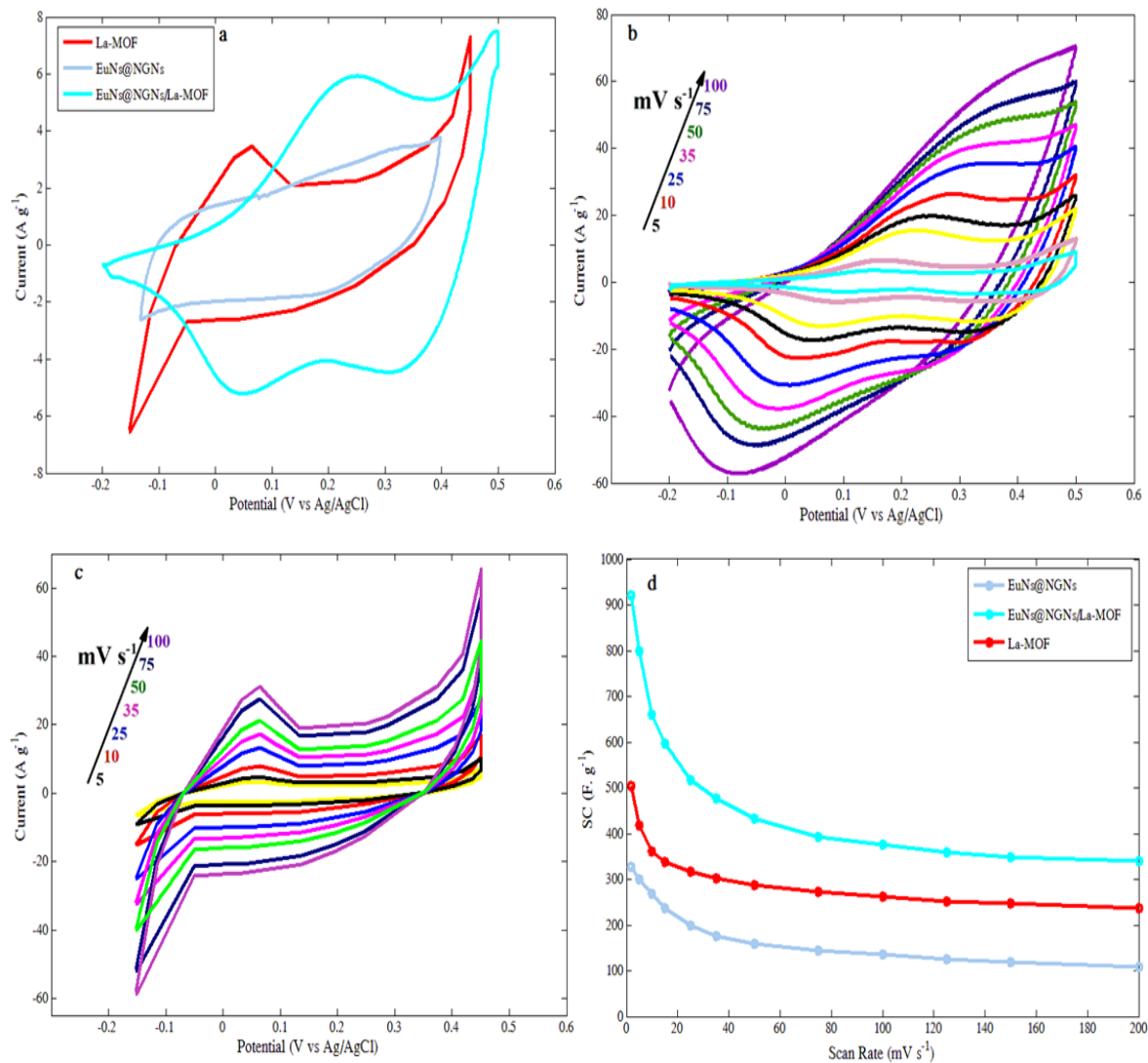


**Figure 6.** Electrochemical properties of electrodes measured using a three-electrode system in 6.0 M KOH aqueous electrolyte. a) CV curves of EuNs@NGNs, La-MOF and EuNs@NGNs/La-MOF electrodes recorded at a scan rate of 2 mV s$^{-1}$, b,c) CV curves of EuNs@NGNs/La-MOF nanocomposite and La-MOF electrode at different scan rates ranging from 2 to 100 mV s$^{-1}$ d) specific capacitance for electrodes at different scan rates

The electrochemical capacitance of supercapacitors composed of metal oxides originates from the redox reactions of oxidations on the electrode. In aqueous solution, europium oxide nanostructures show a transition between three positive and four positive charges in a mutant manner. These transitions, which are accompanied by exchanging protons/cations with the electrolyte, according to the below equation.

$$\text{Eq 5:} \qquad EuO_2 + M^+ + e^- \leftrightarrow EuOOM$$
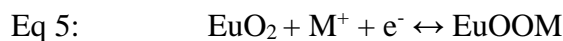
In which M is a $H_3O^+$ or alkaline cations (like $K^+$, $Na^+$). According to the above reversible electron transfer reaction, the calculated specific capacitance for EuNs@NGNs is in terms of redox mechanism [57]. In a hybrid structure like EuNs@NGNs the thin MOF nanosheets offer large surfaces having plentiful channels for quick transfer of ions, and the conducive NGNs allow for fast electron transfer [58]. The specific capacitance (SC) of a chemically active substance can be estimated based on Equation 1. In the course of charging, $EuO_2$ is oxidized to EuOOM, while the discharge involves the reduction of EuOOM to $EuO_2$. The area under the cyclic voltammetry curve for EuNs@NGNs is smaller than the EuNs@NGNs/La-MOF nanocomposite. For Europium Oxide Nanocoparticles decorated on Nitrogen Doped Graphene-MOF, the increase in current can be due to the synergistic effect of combining Europium Oxide with Nitrogen Doped Graphene and MOF and the uniform distribution of europium oxide on N-doped graphene layers and also facilitate the transfer of electrolyte ions through the bulk structures and lattice channels of La-MOF which indicating the EuNs@NGNs/La-MOF nanocomposite shows better supercapacitor properties than EuNs@NGNs or NGNs. Also, the calculated specific capacitance for EuNs@NGNs/La-MOF and EuNs@NGNs are 920 and 328 $F.g^{-1}$ at scanning rate of 2 mV/s, respectively. The capacitance for the MOF electrode is about 505 $F.g^{-1}$. The reduction of the specific capacitance with scan can be seen in Figure 6d. In this diagram, the respective specific capacitance values for EuNs@NGNs and EuNs@NGNs/La-MOF electrodes vary from 328 to 108 $F.g^{-1}$; and 920 to 340 $F.g^{-1}$ upon increasing the scan rate from 2 to 200 mV/s. Also under the same conditions, the MOF electrode had specific capacitance values from 505 to 237 $F.g^{-1}$. Based on these results, at all scanning rates, electrolyte ions are $K^+$ and $H^+$ by mass transporting channels within the lattice structure of the MOF, can be placed in the cavities in the structure of europium oxide nanoparticles decorated on nitrogen- doped graphene nanosheets and boost pseudocapacitive redox reaction and specific capacitance. Hence, EuNs@NGNs/La-MOF electrode has the maximum specific capacitance. Similarly, by increasing the scanning rate to 200 mV/s, this effect of electrolyte ions penetrating in the cavities, due to the limited availability of ion mass transfer to the surface of Europium nanoparticles decreases compared to the initial scanning speeds rates.
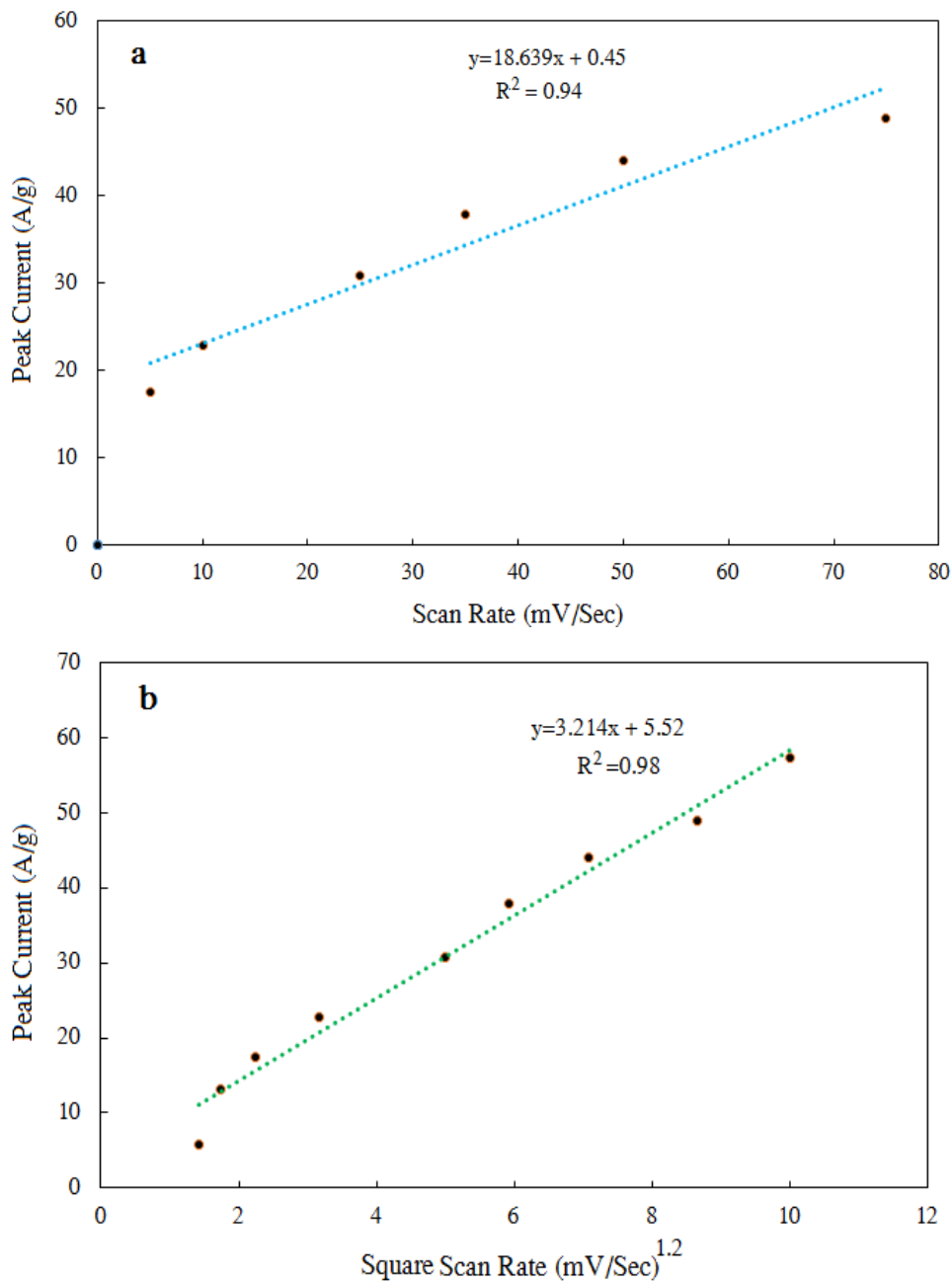
**Figure 7.** Curves of peak current versus a) scan rate b) square scan rate for EuNs@NGNs/La-MOF electrode

Due to the importance of the electroactive surface and its correlation with the behavior of the electrodes, the active surface areas of the prepared electrodes were determined. For this purpose, to determine the electroactive surface of the of EuNs@NGNs/La-MOF nanocomposite, the Randle's-Seick equation was used:

$$\text{Eq 6:} \qquad i_p = 0.4463 nFAC \left(\frac{nFvD}{RT}\right)^{\frac{1}{2}}$$

In this equation $i_p$, and represent the peak current, and number of electrons involved in the electrochemical reaction; F is a Farad constant; A and C represent the specific surface of the supercapacitor and concentration of the electroactive substance; v is the scanning rate; R represents the gas constant; T expresses the temperature in Kelvin; D is the diffusion coefficient of the electroactive species.

The relationship between scanning rate and peak can be used to determine the mechanism of electron transfer. According to Figure 7, if the of the square of the scan rate has a linear relationship with the peak current, the electron transfer mechanism is in the form of penetration into the capacitor.
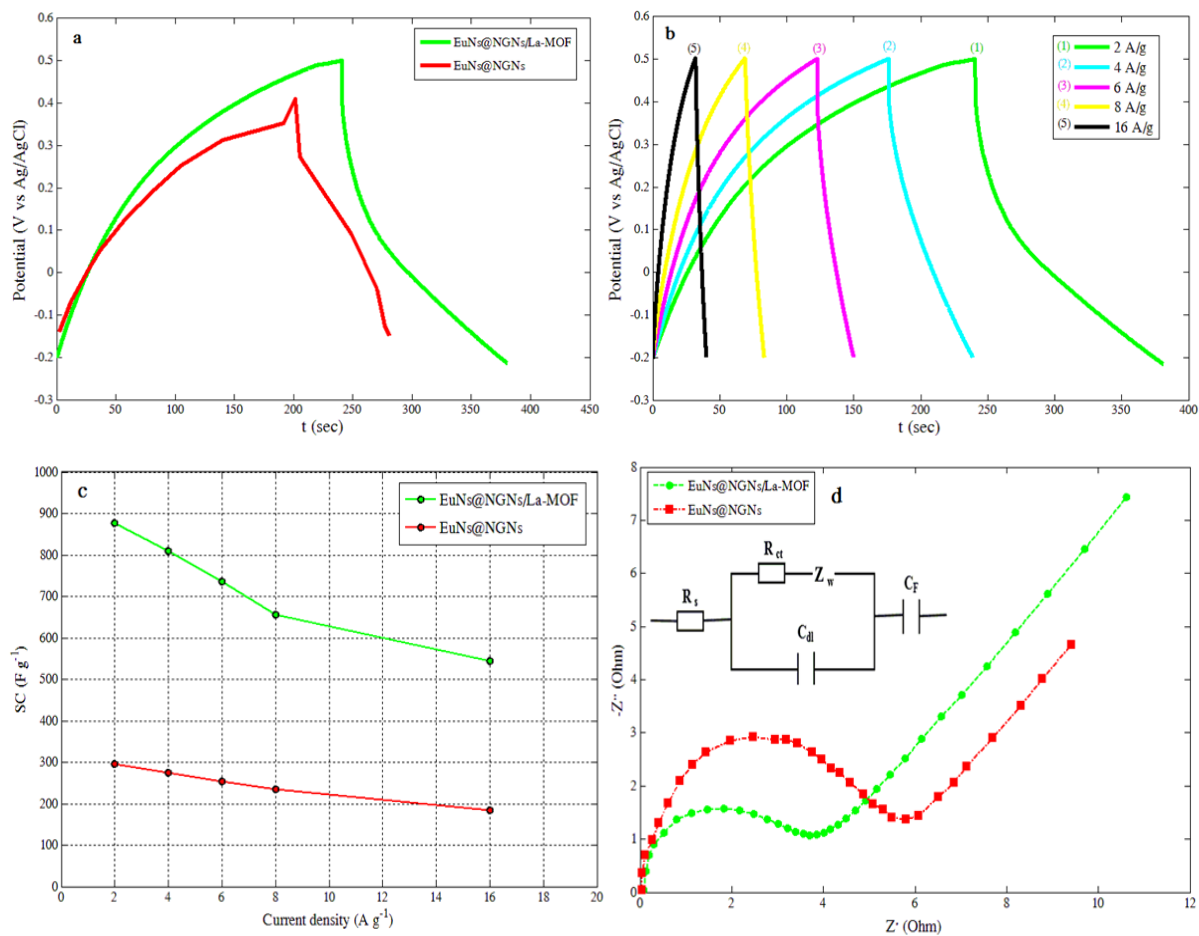


**Figure 8.** Electrochemical properties of electrodes measured using a three-electrode system in 6.0 M KOH aqueous electrolyte; a) galvanostatic charge-discharge of EuNs@NGNs, and EuNs@NGNs/La-MOF electrodes at current density 2 A g$^{-1}$, d) galvanostatic charge-discharge of EuNs@NGNs/La-MOF at different current densities from 2 to 16 A g$^{-1}$, e) specific capacitance for EuNs@NGNs, and EuNs@NGNs/La-MOF electrodes at different current density, f)Electrochemical impedance spectra (EIS) of EuNs@NGNs, and EuNs@NGNs/La-MOF electrodes with insets showing the high-frequency parts

On the other hand, if the peak current has a non-linear relation with the scan rate, the electron transfer mechanism in the supercapacitor is not surface adsorption. This indicates the repeatable and high performance of the supercapacitor at high scan rates. Also, the electroactive surface of the supercapacitor was obtained by extrapolating the equation of Randles-Sevick to 20.2 cm$^2$ per 2 mg of capacitive material. This indicates a very high electroactive surface area for the prepared supercapacitor.

The plots of linear potential changes over time show a symmetrical shape, which is another characteristic that determines an ideal capacitor. There is also no ohmic drop in the electrodes. Good capacitive performance of EuNs@NGNs/La-MOF nanocomposite can be result of high electrical conductivity of nitrogen-doped graphene and reduced internal resistance due to fast mass transfer of the ions in the electrolyte to the electrode surface through metal-organic frameworks channels and even distribution of the nanostructured europium oxide on N-doped graphene. The specific capacitance values recorded for EuNs@NGNs, and EuNs@NGNs/La-MOF nanocomposite electrodesat 2A/g were 295 and 876 F/g. The specific capacitance calculated from the charge-discharge, clearly corresponds with those calculated based on CV results (Figure 8a-c). Discharge time in EuNs@NGNs/La-MOF nanocomposite is longer than EuNs@NGNs, which indicates better supercapacitor performance of this nanocomposite. These curves confirm the obtained data from the cyclic voltammetry method.

**Table 1.** Values obtained from regression of electrochemical impedance spectroscopy data using Levenberg Marquat algorithm and artificial neural networks

|                | EuNs@NGNs | EuNs@NGNs/La-MOF |
|----------------|-----------|------------------|
| $R_s$ (ohm)    | 1.53      | 0.20             |
| $C_{dl}$ (mF)  | 0.42      | 0.53             |
| $R_{ct}$ (ohm) | 5.64      | 3.10             |
| $Z_W$ (mMho)   | 389       | 523              |
| $C_F$ (mF)     | 429       | 592              |

Figure 8d shows the Nyquist curve for EuNs@NGNs, and EuNs@NGNs/La-MOF electrodes in 6.0 M potassium hydroxide solution, in the frequency window of 0.01 to 100 kHz and potential 0.2 volts. Two frequency-dependent regions were noticed at high and frequencies. the data of the high frequency zone, can be used to determine the electrode's internal resistance, as well as the charge transfer resistance of the system. The intercept of the diagram at zero imaginary resistance ($Z_{im}$) shows the internal resistance of the system, also known as equivalent

series resistance. This resistor includes a series combination of electrolyte resistance ($R_S$), electrolyte / electrode contact resistance, current collector resistance, electrode / current collector interface surface resistance, and electrode resistance. Electrochemical impedance spectroscopy data were fitted with Levenberg Marquat algorithm using artificial neural network regression and the results (Table 1) complied with those results obtained by voltametric methods. The equivalent circuit of the measured impedance spectra is shown in Figure 7d. The equivalent circuit consists of 5 elements. The internal resistance (electrolyte solution resistance) $R_s$ is connected in series to the element $C_{dl}$ (electrical double layer capacitance at the electrode/electrolyte interface), which is parallel to the charge transfer resistance ($R_{ct}$) and Warburg impedance. $R_{ct}$ is the result of the kinetic resistance against the ion transfer beween the electrode and the electrolyte or the inherent resistance of the electrode for charge transfer. $Z_w$ is caused by the penetration of the electrolyte cations into the electrode. $C_F$, which is series to the above set, has been used as a measure of the capacitance due to the faradic reaction [59,60].

As can be seen, the Nyquist curve has a large semicircle for both electrodes, indicating the Faraday charge transfer resistance. At low frequencies, $Z_w$ changes with the resistance due to the restriction of electrolyte ion transfer to the electrode cavities. The Nyquist curve is also close to the vertical axis, which indicates the similarity of the electrochemical properties with those of ideal capacitors. The EuNs@NGNs/La-MOF electrode showed the highest $C_{dl}$ and $F_C$ and the lowest $R_{ct}$ compared to EuNs@NGNs electrode. The charge transfer resistance for EuNs@NGNs, and EuNs@NGNs/La-MOF electrodes is 5.64 and 3.10 ohms, respectively. The charge transfer resistance for EuNs@NGNs/La-MOF is less than EuNs@NGNs. The lower charge transfer resistance of EuNs@NGNs/La-MOF nanocomposite is due to its heterogeneous nitrogen and the synergistic effect of Europium Oxide nanostructures and MOF metal framework. The effect of MOF, in addition to providing a large surface area, hosting numerous active sites for the faradic process, improves the power density of the nanocomposite. The improvement in power density according to equation 7 is related to the equivalent series resistance:

$$\text{Eq 7:} \qquad P = \frac{V^2}{4\,R}$$

In this equation, R expresses the equivalent series resistance obtained from the electrochemical impedance diagram, and V represents the applied voltage.
According to this formula, the presence of nitrogen heteroatoms and europium oxide nanostructures as well as MOF improves the electrical conductivity, reducing the equivalent series resistance, and improving the power density [61,62].

The capacitive profile of the nanocomposite, the slope of the low-frequency region, which has a linear region, is obtained, and then the phase angle is determined from the value of this slope through the inverse cotenant.

**Table 2.** Comparison table of EuN@NGNs/La-MOF electrode with other reported works in literatures

| Active materials | Capacitance F g$^{-1}$ (specific current A g$^{-1}$) | Cycle Stability% (cycle number) | Energy density (Wh. kg$^{-1}$) | Ref. |
|---|---|---|---|---|
| $MnO_2$/rGO | 135 (1) | 92 (1000) | 24 | [65] |
| $MnO_2$-NHCS | 392(0.5) | 100 (4000) | 26.8 | [66] |
| $MnO_2$/HCS-30 | 255 (1) | 93.9(5000) | 41.4 | [67] |
| HPCS-$MnO_2$ | 476.4 | 82.1(4000) | 60.8 | [68] |
| g-$C_3N_4$/NiAl-LDH | 714 (0.5) | 82 (10000) | - | [69] |
| $Co_xNi_{1-x}$ LDH/$CN_x$@NGHSs | 1815 (1) | 107.8 (10000) | 28.9 | [70] |
| CC@$NiCo_2Al_x$-LDH | 1137 (0.5) | 91.2 (15000) | 44 | [71] |
| CoAlNi LDH | 1339.6 (1) | 82.2 (3000) | 50.3 | [72] |
| $CoS_x$/Ni-Co LDH | 1562 (1) | 94.56 (10000) | 35.8 | [73] |
| $MnO_2$@C | 756.2 | 100 (5000) | 34.56 | [74] |
| NiHPi-500 | 502 (0.5) | 100 (5000) | 50 | [75] |
| $ZnV_2O_6$@PPy | 723.6 (1) | 93 (3000) | 34 | [76] |
| $Co_3V_2O_8$/$CN_x$ | 1236 (1) | 87 (4000) | 40.83 | [77] |
| Ce-$SnO2$/g-C3N4 | 274 (1) | 84.2 (5000) | 39.3 | [78] |
| g-C3N4/CoAl-LDH | 343 (5) | 93 (6000) | 61.15 | [79] |
| Methylen blue functionalized graphene | 517 (0.5) | 91 (2000) | 30.36 | [80] |
| N,O doped Carbon | 292 (0.5) | 87 (5000) | 18 | [81] |
| Poly (3,4-ethylenedioxypyrrole) with $Fe_3O_4$ or $Co_3O_4$ | 673 (1) | 83 (5000) | 93 | [82] |
| 3D porous g-$C_3N_4$@$V_2O_5$ | 457 (0.5) | 84 (500) | - | [83] |
| PANI-RGO-ZnO | 40 (0.05) | 86 (5000) | 5.61 | [84] |
| Europium oxide nanorod-rGO | 345 (2) | 96.8 (5000) | 35.8 | [49] |
| EuN@NGNs/La-MOF | 876 (2) | 96.2 (2500) | 59 | This work |

The proximity of this phase angle to 90 degrees means the system behavior is near ideal:

$$\text{Eq 8:} \qquad \theta = ArcTg(\frac{Zi}{Zr})$$

The phase angle at the low frequency region is 84 degrees, which is the value of 90 degrees [63].
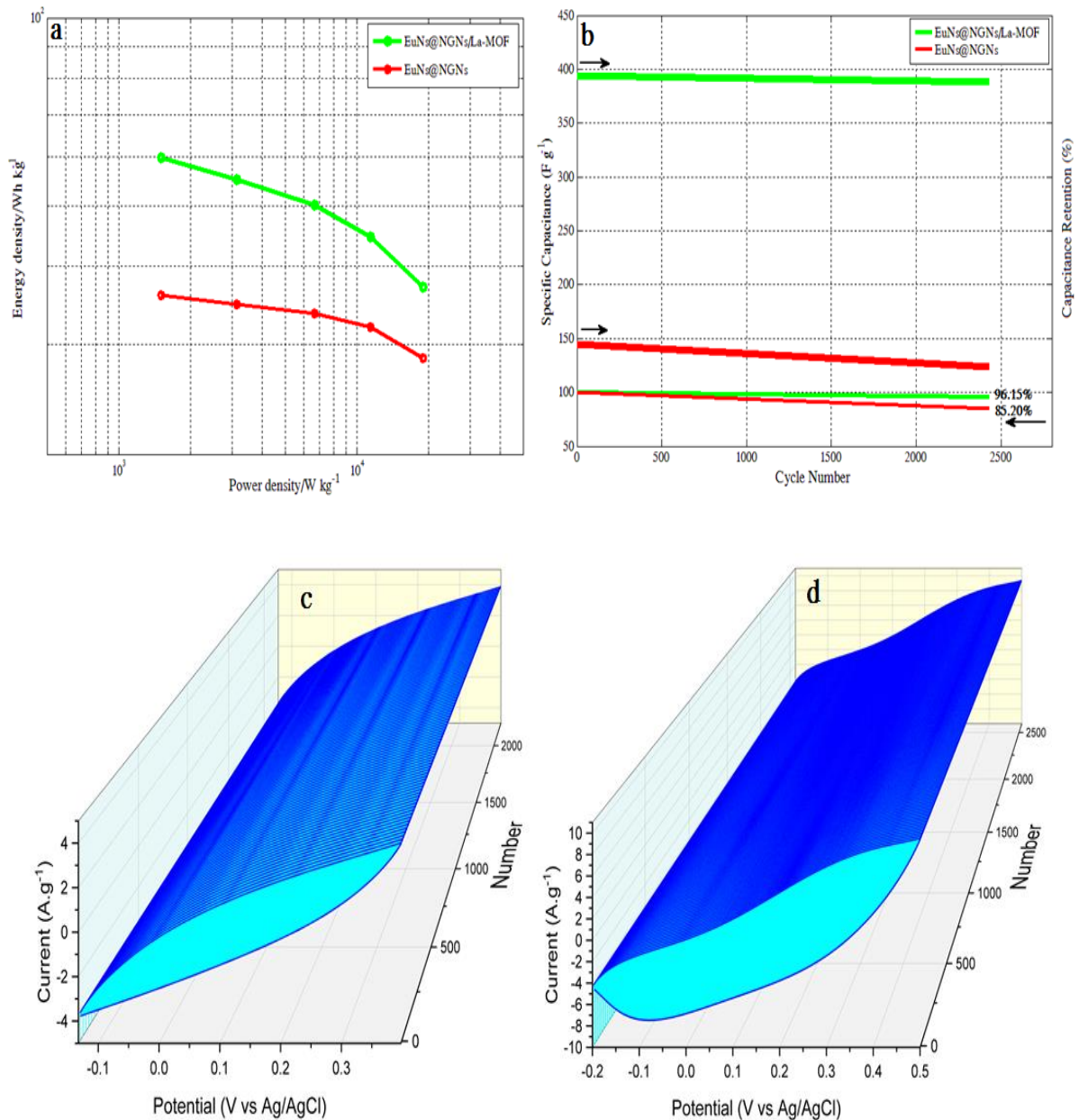


**Figure 9.** a) Ragon Plots of EuNs@NGNs, and EuNs@NGNs/La-MOF b) specific capacitance changes at 75 mV s⁻¹

In the case of EuNs@NGNs, and EuNs@NGNs/La-MOF electrodes the values of the specific capacity were 85.20% and 96.15% of the initial value, indicating the stability of the electrodes during successive cycles has been improved by the composite of Europium Oxide nanostructures to nitrogen-doped graphene/MOF nanocomposite in this method [64]. Therefore, the prepared electrodes have good stability as supercapacitor electrodes.

As two key factors, specific energy (E) and power (P) are used to evaluate supercapacitors performance. Based on the Ragone curve (Figure 9a) EuNs@NGNs/La-MOF electrodes offer high a specific energy value of 59.62 Wh kg$^{-1}$ at 1511 W kg$^{-1}$. Besides, it can be kept specific energy of 37.09 Wh kg$^{-1}$ even at a high specific power of 20000 W kg$^{-1}$. The EuNs@NGNs/La-MOF nanocomposite has higher or similar, specific capacitance, energy and power values to those of reports on recent asymmetric supercapacitors (Table 2).

## 4. CONCLUSION

A new EuNs@NGNs/La-MOF nanocomposite was prepared through a facile sonochemical procedure and the following were concluded:

1. $Eu_2O_3$ nanostructures were evenly decorated on N-doped graphene layers.
2. The EuNs@NGNs/La-MOF electrode had higher specific capacitance, current response and electrochemical active area than EuNs@NGNs electrode.
3. In such hybrid structure the NGNs support, facilitates fast electron transfer, while ultrathin MOF sheets create large surfaces hosting numerous channels for transfer of electrolyte ions includes $K^+$ and $H^+$ by mass transporting channels within the lattice structure of the MOF, which can be placed in the cavities in the structure of Europium oxide nanoparticles.
4. The specific capacitance for EuNs@NGNs, and EuNs@NGNs/La-MOF nanocomposite at 2A/g is 295 and 876 F/g respectively, which complies with the results obtained through cyclic voltammetry.
5. Based on EIS results, EuNs@NGNs/La-MOF electrode showed the highest $C_{dl}$ and $F_C$ and the lowest $R_{ct}$ compared to EuNs@NGNs electrode. The charge transfer resistance for EuNs@NGNs, and EuNs@NGNs/La-MOF electrodes is 5.64 and 3.10 ohms, respectively.
6. The EuNs@NGNs/La-MOF electrodes offer a high specific energy value of 59.62 Wh kg$^{-1}$ at 1511 W kg$^{-1}$, and maintains its specific energy of 37.09 Wh kg$^{-1}$ even at a high specific power of 20000 W kg$^{-1}$. This reflects the promise of the application of the material in high-performance CSs.

**Conflicts of interest**

There are no conflicts of interest to declare.

**Acknowledgement**

The authors are very thanks to the University of Tehran, the Center of Excellence in Electrochemistry, for supporting facilities to bring about this work by Major Research Project.

**REFERENCES**

[1]    W. Li, B. Zhang, R. Lin, S. Ho-Kimura, G. He, X. Zhou, J. Hu, and I.P. Parkin, Advanced Functional Materials 28 (2018) 1705937.

[2]    C.V.M. Gopi, R. Vinodh, S. Sambasivam, I.M. Obaidat, and H.J. Kim, Journal of Energy Storage 27 (2020) 101035.

[3]    Y. Ge, Z. Liu, Y. Wu, and R. Holze, Electrochimica Acta 366 (2021) 137390.

[4]    K.V.G. Raghavendra, R. Vinoth, K. Zeb, C.V.M. Gopi, S. Sambasivam, M.R. Kummara, I.M. Obaidat, and H.J. Kim, Journal of Energy Storage 31 (2020) 101652.

[5]    G. Wang, L. Zhang, and J. Zhang, Chemical Society Reviews 41 (2012) 797.

[6]    L. Jiang, M. Yao, B. Liu, Q .Li, R. Liu, H. Lv, S. Lu, C. Gong, B. Zou, T. Cui, The Journal of Physical Chemistry C 116 (2012) 11741.

[7]    A.G. Pandolfo, and A.F. Hollenkamp, Journal of Power Sources, 157 (2006) 11.

[8]    Y. Wang, C.X. Guo, J. Liu, T. Chen, H. Yang, and C.M. Li, Dalton Transactions 40 (2011) 6388.

[9]    Z.S. Wu, G. Zhou, L.C. Yin, W. Ren, F. Li, and H.M. Cheng, Nano Energy 1 (2012) 107.

[10]   H. Pourfarzad, R. Badrnezhad, M. Ghaemmaghami, and M. Saremi, Ionics (2021).

[11]   E. Bassey, L. Yang, M. Cao, Y. Feng, and J. Yao, Journal of Electroanalytical Chemistry (2020) 114972.

[12]   T. He, X. Li, Y. Wang, T. Bai, X. Weng, and B. Zhang, Journal of Electroanalytical Chemistry 878 (2020) 114597.

[13]   Y. Shabangoli, M.S. Rahmanifar, A. Noori, M.F. El-Kady, R.B. Kaner, and M.F. Mousavi, ACS Nano 13 (2019) 2567.

[14]   A. Asghari, S.H. Kazemi, and M. Khanmohammadi, Journal of Materials Science: Materials in Electronics 31 (2020) 4354.

[15]   F. Bahmani, S.H. Kazemi, H. Kazemi, M.A. Kiani, and S.Y. Feizabadi, Journal of Alloys and Compounds 784 (2019) 500.

[16]   S.H. Kazemi, A. Asghari, and M.A. kiani, Electrochimica Acta 138 (2014) 9.

[17]   B. Mordina, N.S. Neeraj, A.K .Srivastava, K. Mukhopadhyay, and N.E. Prasad, Journal of Electroanalytical Chemistry (2020) 114850.

[18] H.-J. Kim, D-.J. Kim, T. Anitha, A.k. Yedluri, J.-S. Bak, I. Cho, M. Jagadeesh, and A.E. Reddy, New Journal of Chemistry 43 (2019) 15605.

[19] Y. Anil Kumar, S. Singh, D.K. Kulurumotlakatla, and H.J. Kim, New Journal of Chemistry 44 (2020) 522.

[20] Y. Shabangoli, M.S. Rahmanifar, M.F. El-Kady, A. Noori, M.F. Mousavi, and R.B. Kaner, Energy Storage Materials 11 (2018) 282.

[21] H. Pourfarzad, M. Shabani-Nooshabadi, M.R. Ganjali, and H. Kashani, Electrochimica Acta 317 (2019) 83.

[22] H. Khammar, A. Abdelwahab, H.S. Abdel-Samad, and H.H. Hassan, Journal of Electroanalytical Chemistry (2020) 114848.

[23] S. Zheng, X. Li, B. Yan, Q. Hu, Y. Xu, X. Xiao, H. Xue, and H. Pang, Advanced Energy Materials 7 (2017) 1602733.

[24] J. Yang, X. Xiao, P. Chen, K. Zhu, K. Cheng, K. Ye, G. Wang, D. Cao, and J. Yan, Nano Energy 58 (2019) 455.

[25] J. Li, Y. Wang, W. Xu, Y. Wang, B. Zhang, S. Luo, X. Zhou, C. Zhang, X. Gu, and C. Hu, Nano Energy 57 (2019) 379.

[26] C. Sengottaiyan, R. Jayavel, R.G. Shrestha, T. Subramani, S. Maji, J.H. Kim, J.P. Hill, K. Ariga, and L.K. Shrestha, Bulletin of the Chemical Society of Japan 92 (2019) 521.

[27] J. Zhang ,Z. Zhang, Y. Jiao, H. Yang, Y. Li, J. Zhang, and P. Gao, Journal of Power Sources 419 (2019) 99.

[28] D. Joung, and S.I. Khondaker, Physical Review B 86 (2012) 235423.

[29] F. Wang, X. Wu, X. Yuan, Z. Liu, Y. Zhang, L. Fu, Y. Zhu, Q. Zhou, Y. Wu, and W. Huang, Chemical Society Reviews 46 (2017) 6816.

[30] C.R. Mulzer, L. Shen, R.P. Bisbey, J.R. McKone, N. Zhang, H.C.D. Abruña, and W.R. Dichtel, ACS Central Science 2 (2016) 667.

[31] L. Wang, Y. Han, X. Feng, J. Zhou, P. Qi, and B. Wang, Coordination Chemistry Reviews 307 (2016) 361.

[32] H. Pourfarzad, M. Shabani-Nooshabadi, and M.R. Ganjali, Journal of Power Sources 451 (2020) 27768.

[33] H.B. Wu, and X.W.D. Lou, Science Advances 3 (2017) eaap9252.

[34] M. Khan, M.N. Tahir, S.F. Adil, H.U. Khan, M.R.H. Siddiqui, A.A. Al-warthan, and W. Tremel, Journal of Materials Chemistry A 3 (2015) 18753.

[35] T. Van Ngo, M. Moussa, T.T. Tung, C. Coghlan, and D. Losic, Electrochimica Acta 329 (2020) 135104.

[36] H. Zhang, D. Yang, A. Lau, T. Ma, H. Lin, and B. Jia, Small 17 (2021) 2007311.

[37] R.K. Singh, R. Kumar, D.P. Singh, R. Savu, and S.A. Moshkalev, Materials Today Chemistry 12 (2019) 282.

[38] R. Kumar, A.V. Alaferdov, R.K. Singh, A.K. Singh, J. Shah, R.K. Kotnala, K. Singh, Y. Suda, and S.A. Moshkalev, Composites Part B 168 (2019) 66.

[39] R. Kumar, S. Sahoo, E. Joanni, R.K. Singh, K. Maegawa, W.K. Tan, G. Kawamura, K.K. Kar, and A. Matsuda, Materials Today 39 (2020) 47.

[40] D.A. Johnson, Journal of Chemical Education 57 (1980) 475.

[41] R.B. Rakhi, W. Chen, D. Cha, and H.N. Alshareef, Journal of Materials Chemistry 21 (2011) 16197.

[42] A.S. Dezfuli, M.R. Ganjali, H.R. Naderi, and P. Norouzi, RSC Advances 5 (2015) 46050.

[43] H. Jafari, M.R. Ganjali, A. Shiralizadeh Dezfuli, and E. Kohan, Journal of Materials Science: Materials in Electronics 29 (2018) 20639.

[44] L. Sun, D. Li, H. Du, J. Zhu, L. Hu, and D. Guo, International Journal of Hydrogen Energy 46 (2021) 3974.

[45] Z. Sun, D.K. James, and J.M. Tour, The Journal of Physical Chemistry Letters 2 (2011) 2425.

[46] W. Ai, W. Zhou, Z. Du, Y. Du ,H. Zhang, X. Jia, L. Xie, M. Yi, T. Yu, and W. Huang, Journal of Materials Chemistry 22 (2012) 23439.

[47] M. Hosseini, M.R.K. Pur, P. Norouzi ,M.R. Moghaddam, and M.R. Ganjali, Materials Science and Engineering: C 76 (2017) 483.

[48] A. Ambrosi, A .Bonanni, Z. Sofer, J.S. Cross, and M. Pumera, Chemistry–A European Journal 17 (2011) 10763.

[49] P. Aryanrad, H.R. Naderi, E. Kohan, M.R. Ganjali, M. Baghernejad, and A.S. Dezfuli, RSC Advances 10 (2020) 17543.

[50] N. Van Hoa, P.A. Dat, N. Van Hieu, T.N. Le, N.C. Minh, N. Van Tang, D.T. Nga, and T.Q. Ngoc, Diamond and Related Materials 106 (2020) 107850.

[51] Z. Çıplak, A. Yıldız, and N. Yıldız, Journal of Energy Storage 32 (2020) 101846.

[52] G. Santhosh, annd A.S. Bhatt, Graphene and Graphene-Integrated Materials for Energy Device Applications, Monoelements: Properties and Applications (2020) pp. 285.

[53] M. Zhou, X. Li, J. Cui, T. Liu ,T. Cai, H. Zhang, and S. Guan, Int. J. Electrochem. Sci. 7 (2012) 9984.

[54] T.N. Huan, T. Van Khai, Y. Kang ,K.B. Shim, and H. Chung, Journal of Materials Chemistry 22 (2012) 14756.

[55] M. Sathish, S. Mitani, T. Tomai, and I. Honma, Journal of Materials Chemistry A 2 (2014) 4731.

[56] L. Jiang, M. Yao ,B. Liu, Q. Li, R. Liu, Z. Yao, S. Lu, W. Cui, X. Hua, and B. Zou, CrystEngComm 15 (2013) 3739.

[57] C.C. Hu, and T.W. Tsou, Electrochemistry Communications 4 (2002) 105.

[58] L.G. Beka, X. Bu, X. Li, X. Wang, C. Han, and W. Liu, RSC Advances 9 (2019) 36123.

[59] S. Sanati, Z. Rezvani, Chemical Engineering Journal, 362 (2019) 743.

[60] H.R. Naderi, M.R .Ganjali, A.S. Dezfuli, Journal of Materials Science: Materials in Electronics 29 (2018) 3035.

[61] Q.F. Wu, K.X. He, H.Y. Mi, and X.G. Zhang, Materials Chemistry and Physics 101 (2007) 367.

[62] L. Que, L. Zhang, C. Wu, Y. Zhang, C. Pei, F. Nie, Pt-decorated graphene network materials for supercapacitors with enhanced power density, Carbon, 145 (2019) 281.

[63] H.K. Song, H.Y. Hwang, K.H. Lee, L.H. Dao, Electrochimica Acta 45 (2000) 2241.

[64] P. Norouzi, M. Ganjali, S. Labbafi, A. Mohammadi, Analytical letters 40 (2007) 747.

[65] E. Miniach, A. Śliwak, A. Moyseowicz, L. Fernández-Garcia, Z. González, M. Granda, R. Menendez, and G. Gryglewicz, Electrochimica Acta 240 (2017) 53.

[66] T. Liu, C. Jiang, W. You, and J. Yu, Journal of Materials Chemistry A 5 (2017) 8635.

[67] W. Du, X. Wang, J. Zhan, X. Sun, L. Kang, F. Jiang, X. Zhang, Q. Shao, M. Dong, H. Liu, V. Murugadoss, and Z. Guo, Electrochimica Acta 296 (2019) 907.

[68] X. Yuan, Y. Zhang, Y. Yan, B. Wei, K. Qiao, B. Zhu, X. Cai, T.-W. Chou, Chemical Engineering Journal (2019).

[69] L. Zhang, M. Ou, H. Yao, Z. Li, D. Qu, F. Liu, J. Wang, J. Wang, and Z. Li, Electrochimica Acta 186 (2015) 292.

[70] X. Hao, Z. Jiang, X. Tian ,X. Hao, and Z.J. Jiang, Electrochimica Acta 253 (2017) 21.

[71] X. Gao, X. Liu, D. Wu ,B. Qian, Z. Kou, Z. Pan, Y. Pang, L. Miao, and J. Wang, Advanced Functional Materials 29 (2019) 1903879.

[72] H. Chen, H. Zhang, Y. Zhang, Y. Wang, X. Su, L. Zhang, and Z. Lin, Chemical Engineering Journal 375 (2019) 121926.

[73] X. Guan, M. Huang ,L. Yang, G. Wang, X. Guan, Chemical Engineering Journal, 372 (2019) 151.

[74] Y. Xie, C. Yang, P. Chen, D. Yuan, K. Guo, Journal of Power Sources, 425 (2019) 1.

[75] N.L. Wulan Septiani, Y.V. Kaneti, K.B. Fathoni, J. Wang, Y. Ide, B. Yuliarto, Nugraha, H.K. Dipojono, A.K. Nanjundan, D. Golberg, Y. Bando, Y. Yamauchi, Nano Energy, 67 (2020) 104270.

[76] L. Halder, A. Kumar Das, A. Maitra, A. Bera, S. Paria, S.K. Karan, S.K. Si, S. Ojha, A. De, and B.B. Khatua, New Journal of Chemistry 44 (2020) 1063.

[77] R. Mishra, P. Panda, S. Barman, New Journal of Chemistry45 (2021) 5897.

[78] S. Asaithambi, P. Sakthivel, M. Karuppaiah, R. Yuvakkumar, D. Velauthapillai, T. Ahamad, M.A.M. Khan, M.K.A. Mohammed, N. Vijayaprabhu, and G. Ravi, Journal of Alloys and Compounds, 866 (2021) 158807.

[79] S. Sanati, and Z. Rezvani, Chemical Engineering Journal, 362 (2019) 743.

[80] L. Deng, C. Zhou, Z. Ma, and G. Fan, Journal of Colloid and Interface Sci. 561 (2020) 416.

[81]   L. Zhang, L. Xu, Y. Zhang, X. Zhou, L. Zhang, A. Yasin, L. Wang, K. Zhi, RSC Advances 8 (2018) 3869.

[82]  B.N. Reddy, S. Deshagani, M. Deepa, and P. Ghosal, Chemical Engineering Journal 334 (2018) 1328.

[83]  Y. Zhou, L .Sun, D. Wu, X. Li, J. Li, P. Huo, H. Wang, and Y. Yan, Journal of Alloys and Compounds 817 (2020) 152707.

[84]  S. Palsaniya, H.B. Nemade, and A.K. Dasmahapatra, J. Physics Chem. Solids 154 (2021) 110081.